Role of bromine in restoring superconductivity in $YBa_2Cu_3O_y$

D. M. Potrepka, J. I. Budnick, D. B. Fenner,* and W. A. Hines
Department of Physics and Institute of Materials Science, University of Connecticut, Storrs, Connecticut 06269

M. Balasubramanian
Chemical Technology Division, Argonne National Laboratory, Argonne, Illinois 60439

A. R. Moodenbaugh
Materials Science Division, Brookhaven National Laboratory, Upton, New York 11973
(Received 5 April 1999)

^{63,65}Cu nuclear quadrupole resonance (NQR), ^{63,65}Cu and ^{79,81}Br nuclear magnetic resonance (NMR), and Br *K*-edge x-ray-absorption fine-structure (XAFS) measurement techniques have been used to study the local structures of Cu and Br in well-characterized samples of deoxygenated and brominated $YBa_2Cu_3O_y$ (YBCO). The combined results provide a detailed picture of the role of bromine in reoxygenating the YBCO structure and an explanation for the partial restoration of superconductivity in the YBCO system. Characterization of the powder samples, with particle sizes of 1, 20, 30, and 40 μm, included x-ray diffraction, thermal gravimetric analysis, energy dispersive x-ray analysis, and magnetometry. From the XAFS and NMR results, it is concluded that, upon bromination at 260 °C, Br does not enter the YBCO lattice either substitutionally or interstitially. Instead, there is compelling evidence for the formation of nanoscale $BaBr_2$ precipitates which result from the local destruction of the $YBa_2Cu_3O_y$ phase. Furthermore, on the basis of the NQR and NMR experiments, it is concluded that through this decomposition into an inhomogeneous material, oxygen is liberated which repopulates the nearby O(4) chain sites, thus restoring superconductivity. [S0163-1829(99)01838-X]

I. INTRODUCTION

In studies involving the halogenation of $YBa_2Cu_3O_y$ (YBCO), it has been observed that Cl,[1] Br,[2–6] and I[7] return the lattice of deoxygenated YBCO from the nonsuperconducting tetragonal phase to the orthorhombic phase with superconductivity being partially restored. In particular, Radousky *et al.*[2] report that the partially restored phase that results from the bromination of deoxygenated YBCO yields a reduced critical current J_c, compared to that of the fully oxygenated parent $YBa_2Cu_3O_{7-\delta}$. In addition, the magnetic-field dependence of J_c which has been observed for such brominated materials has stimulated interest because of potential application in flux-flow studies.[5,8] The location of the Br atoms in the treated material and its effect on the restoration of superconductivity in deoxygenated YBCO remained unexplained until very recently.[6] Presented here is a more thorough investigation into the structural properties of brominated YBCO. This study provides a detailed picture of the role of bromine in the partial decomposition of deoxygenated YBCO and the restoration of superconductivity in the undecomposed regions of the deoxygenated phase.

Halogens are known to cause some degradation of the YBCO superconductor.[1–5,7] X-ray photoelectron spectroscopy binding-energy studies reported by Fukuda *et al.*[9] indicate that bromine inserted into deoxygenated YBCO may have a chemical environment similar to that in $BaBr_2$. However, the x-ray photoelectron spectroscopy technique is surface sensitive and may not represent the bulk composition. Their assumptions are, however, also supported by their Raman and magnetometry studies. Neutron-diffraction measurements suggest that the Br atoms occupy vacant O(4) sites in the YBCO lattice, although such experiments are hampered by the similarity in the neutron-scattering lengths of oxygen and bromine.[4] Also, the broadening of x-ray-diffraction peaks has been attributed to Br atoms occupying the interstitial sites in the YBCO lattice;[1] however, no direct evidence exists for this to date. Kemnitz *et al.*[10] have suggested that another halogen, Cl, which partially restores superconductivity in $YBa_2Cu_3O_{6.3}$, causes a local decomposition reaction to occur, creating an amorphous product and simultaneously oxygenating the unreacted grain interiors. The amorphous nature and nonsuperconducting behavior of much of the resulting sample for high Cl content are seen as evidence for a partial decomposition. They interpret the incorporation of a large amount of chlorine into YBCO as inconsistent with an otherwise unchanged YBCO structure. Studies of chlorine addition to $YBa_2Cu_3O_{6.2}$ by Faulques *et al.*[11] using x-ray photoelectron spectroscopy and x-ray diffraction indicate that the Cl oxidation number is between -1 and 0. This led to the conclusion that chlorine enters vacancies in BaO planes and promotes diffusion of the oxygen toward empty O(1) sites, a conclusion that was also supported by Raman spectroscopy results.

In order to understand the mechanism by which superconductivity is restored, it is important to understand the local atomic structures of Cu and Br in the brominated YBCO system. In this work, nuclear quadrupole resonance (NQR) and nuclear magnetic resonance (NMR) of ^{63,65}Cu, NMR of ^{79,81}Br, and x-ray-absorption fine-structure (XAFS) of the Br *K*-edge were utilized to study the local structure in well-characterized powder samples of parent, deoxygenated, and brominated $YBa_2Cu_3O_y$. The sample characterization included: (1) thermal gravimetric analysis (TGA) to measure

TABLE I. Samples and characteristics.

Sample	Composition	Preparation	T_{max}(K)	T_c(K)	$(M/M_p)_{10\ K}$	MFR(%)
S1	$YBa_2Cu_3O_{6.9}$	1 μm; parent	86	92	1.00	6.1
S2	$YBa_2Cu_3O_{6.9}+Br_2$	Br_2 260 °C, $\frac{1}{2}$ h	86	92	1.00	6.1
S3	$YBa_2Cu_3O_{6.6}$	He 450 °C, 4 h	48	60	0.26	1.6
S4	$YBa_2Cu_3O_{6.6}+Br_2$	He 450 °C, 4h; Br_2 260 °C, $\frac{1}{2}$ h	86	92	0.52	3.2
S5	$YBa_2Cu_3O_{6.1}$	He 700 °C, 4 h	<5	<5	0	0
S6	$YBa_2Cu_3O_{6.1}+Br_2$	He 700 °C, 4 h; Br_2 260 °C, $\frac{1}{2}$ h	86	92	0.35	2.1
S7	$YBa_2Cu_3O_{6.2}$	He 675 °C, 8 h				
S8	$YBa_2Cu_3O_{6.2}$	He 675 °C, 8 h; vac. 260 °C, $\frac{1}{2}$ h				
S9	$YBa_2Cu_3O_{6.6}+O_2$	He 450 °C, 4 h; O_2 560 °C, 4 h	87	92	0.85	5.2
L1	$YBa_2Cu_3O_{6.9}$	20 μm; parent	87	93	1.00	7.9
L2	$YBa_2Cu_3O_{6.6}$	He 450 °C, 4 h	57	69	0.42	3.3
L3	$YBa_2Cu_3O_{6.6}+Br_2$	He 450 °C, 4 h; Br_2 260 °C, $\frac{1}{2}$ h	85	92	0.71	5.6
L4	$YBa_2Cu_3O_{6+\delta}$	He 750 °C, 5 h	<5	<5	0	0
L5	$YBa_2Cu_3O_{6+\delta}+Br_2$	He 750 °C, 5 h; Br_2 260 °C, $\frac{1}{4}$ h	85	93	0.48	3.8
M1	$YBa_2Cu_3O_{6.9}$	40 μm; parent	90	93	1.00	100
M2	$YBa_2Cu_3O_{6.7}$	He 450 °C, 4 h	58	80	0.46	46
M3	$YBa_2Cu_3O_{6.7}+Br_2$	He 450 °C, 4 h; Br_2 260 °C, $\frac{1}{2}$ h	90	93	0.85	85
M4	$YBa_2Cu_3O_{6.9}$	30 μm; parent	90	92	1.00	79
M5	$YBa_2Cu_3O_{6.9}+Br_2$	Br_2 260 °C, 24 h	90	92	1.05	83
M6	$YBa_2Cu_3O_{6.1}+Br_2$	He 700 °C, 4 h; Br_2 260 °C, 24 h	82	90	0.18	14

Sample S1 (parent), $M_p = -7.7\times10^{-3}$ emu/g
Sample L1 (parent), $M_p = -1.0\times10^{-2}$ emu/g
Sample M1 (parent), $M_p = -1.3\times10^{-1}$ emu/g
Sample M4 (parent), $M_p = -1.0\times10^{-1}$ emu/g

the oxygen content after deoxygenation, (2) energy dispersive x-ray analysis (EDAX) to monitor the presence of bromine after bromination, (3) x-ray diffraction (XRD) of the parent, deoxygenated, and brominated samples, and (4) superconducting quantum interference device (SQUID) magnetometry to monitor the effect of deoxygenation and bromination on the superconductivity. Values for the nominal oxygen content, which were assigned to the samples after deoxygenation, were obtained primarily from the TGA results; however, for comparison, values were also obtained from measurements of the superconducting transition temperature T_c, and lattice parameters. The Br *K*-edge XAFS experiments on deoxygenated and brominated YBCO clearly demonstrate that bromine does not occupy any detectable number of sites within the YBCO lattice, either as a substitutional or interstitial atom. Instead, the XAFS results indicate the presence of $BaBr_2$ regions with nanoscale dimensions. Furthermore, the ^{79,81}Br NMR measurements show that the local environment surrounding the Br atoms in brominated YBCO is very similar to that for Br in $BaBr_2$. ^{63,65}Cu NQR and NMR spectra obtained from Cu atoms in the chain Cu(1) and plane Cu(2) sites show that the bromination treatment essentially restores the spectra from that characteristic of deoxygenated YBCO to that characteristic for a fully oxygenated parent $YBa_2Cu_3O_{7-\delta}$ superconductor. However, the intensity of the plane Cu(2) peaks relative to the chain Cu(1) peaks in the brominated samples is diminished when compared to those in the parent material. By using three locally probing measurement techniques, NQR, NMR, and XAFS, information has been obtained concerning the structural changes induced by the bromination of deoxygenated $YBa_2Cu_3O_{7-\delta}$ and the nature of the restoration of the superconducting state.

II. EXPERIMENTAL APPARATUS AND PROCEDURE

A. Sample preparation and characterization

Several powder samples were prepared and characterized for use in the NQR, NMR, and XAFS experiments. Table I lists each sample, along with the corresponding composition (nominal oxygen content), particle size, and deoxygenation/bromination treatment. Samples S1 through S9 were prepared from 99.999% pure $YBa_2Cu_3O_{7-\delta}$ parent powder obtained from Superconducting Components, Inc., with an oxygen content $y=7-\delta=6.9\pm0.1$ and 1-μm particle size. Samples L1 through L5 were prepared from 99.999% pure $YBa_2Cu_3O_{7-\delta}$ parent powder obtained from Kurt J. Lesker, Inc., with an oxygen content $y=7-\delta=6.9\pm0.1$ and 20-μm particle size. Finally, samples M1 through M6 were prepared from a $YBa_2Cu_3O_{7-\delta}$ parent powder with oxygen content $y=7-\delta=6.9\pm0.1$ that was fabricated according to published methods.[12] The sample was ground and sieved to obtain parent powders with 40-μm (samples M1–M3) and 30-μm (samples M4–M6) particle size.

Deoxygenation was carried out by heating the sample powder in a chamber which was first evacuated and then filled with 99.999% pure He gas that was allowed to flow through the chamber. Generally speaking, two deoxygen-

ation temperatures were used: (1) the relatively low value of 450 °C and (2) higher values near 700 °C. The deoxygenation time ranged from 4–8 h. At the conclusion of the deoxygenation treatment, the sample powder was allowed to cool to room temperature. Bromination was carried out using an ''equilibrium'' technique based on a method previously employed by Radousky and co-workers.[2,13] In this procedure, the sample chamber was initially evacuated to a background pressure of 2×10^{-6} torr to reduce the effect of contaminants. The sample powder was heated to 260 °C and then exposed to a source containing liquid bromine at room temperature such that during bromination, the total pressure in the sample chamber was just the Br_2 vapor pressure. Upon completion of the bromination treatment, the liquid bromine source temperature was lowered to 77 K by immersing it in liquid N_2, which caused the Br_2 vapor in the sample chamber to be reclaimed at the bromine source. The sample powder was then exposed to an inert He gas flow and cooled to room temperature. The typical bromination treatment time was $\frac{1}{2}$ h. However, a shorter time of $\frac{1}{4}$ h and longer time of 24 h were also used. Table I shows that sample S7, with a 1-μm particle size, was deoxygenated at 675 °C for 8 h. Sample S8 underwent the same deoxygenation treatment as sample S7, and then was exposed to the same thermal treatment used in bromination (260 °C for $\frac{1}{2}$ h) except that it was under vacuum with no Br_2 vapor present.

Estimates for the resulting sample stoichiometry (or nominal oxygen content) after deoxygenation were made (indirectly) using a Perkin-Elmer TGA-7 instrument for thermal gravimetric analysis. Initial TGA measurements using powder samples proved to be uncertain due to large changes in mass during the cooldown following the deoxygenation heat treatment. This was attributed to temperature-dependent surface effects. Consequently, subsequent measurements were carried out on small pieces of bulk $YBa_2Cu_3O_{7-\delta}$ which were approximately cubic, 2 mm on each side. In addition, samples S2, S4, S6, M5, and M6 were analyzed using energy dispersive x-ray analysis in order to monitor the bromine content. X-ray-diffraction measurements were carried out on the various parent powder samples as well as after the deoxygenation and bromination treatments using a Phillips diffractometer equipped with a single crystal monochrometer and Cu-$K\alpha$ radiation ($\lambda=1.5418$ Å). The intensity was recorded as a function of 2Θ, Θ being the Bragg diffraction angle, using a homemade computer interface. Finally, magnetization measurements were performed on the samples listed in Table I using a Quantum Design MPMS SQUID magnetometer.

B. Nuclear quadrupole resonance and nuclear magnetic resonance

^{63,65}Cu NQR and NMR spectra, as well as ^{79,81}Br NMR spectra, were obtained using a Matec phase-coherent spin-echo pulse spectrometer. Details concerning the instrumentation, experimental procedure, and data acquisition are provided in references 13 and 14 and references therein. A conventional double glass dewar system with pumping enabled operation at liquid-He temperatures. In particular, zero-field spin-echo NQR and NMR spectra were obtained for ^{63,65}Cu nuclei in the chain Cu(1) and plane Cu(2) sites in YBCO over the frequency ranges 18–34 MHz and 70–110 MHz. In order to initially approximate the tuning and excitation conditions, the room-temperature ^{63}Cu NQR free induction decay was observed at 26.0 MHz in Cu_2O. For the ^{63,65}Cu spectra, a typical $t_{\pi/2}$-τ-$t_\pi=4$ μs-60 μs-8 μs spin-echo pulse sequence was used with a 0.5-Hz repetition rate. Spectra were obtained with usable signal-to-noise by averaging 100 repetitions. ^{79,81}Br NMR measurements were made using the same phase-coherent pulse spectrometer described above along with an Oxford Instruments superconducting magnet. The frequency was fixed at $\nu=52.84$ MHz as the magnetic field was ramped (swept) from 4.5–5.0 T. For the ^{79,81}Br spectra, a typical $t_{\pi/2}$-τ-$t_\pi=20$ μs-120 μs-40 μs spin-echo pulse sequence was used with a 10-Hz repetition rate. Spectra were obtained with usable signal-to-noise by averaging 5000 repetitions.

C. Extended x-ray-absorption fine structure

The XAFS experiments were carried out in the transmission mode at the X-11A beamline of the National Synchrotron Light Source, Brookhaven National Laboratory, using a double-crystal Si (111) monochromator. This beamline has instrumentation which can be used to make XAFS and fluorescence measurements at the absorption edges of the elements being studied. The apparatus is described in detail elsewhere.[13,15] For each sample, the powder was rubbed onto Kapton tape which was used to create a stack of layers to get an appropriate edge jump and to avoid systematic errors for the thickness effect. Harmonic rejection was accomplished by detuning the monochromator to ~80% of its peak intensity. In this work, experiments to observe the Br *K*-edge were carried out. The measurements were made at room temperature and below; the sample temperature was reduced by two methods. In the first method, the samples were cooled moderately ($T\sim200$ K) by attaching them to a copper holder, the sample remaining in air, while the other end of the holder was exposed to a liquid-nitrogen bath. In the second method, the samples were mounted in a Displex closed-cycle refrigerator resulting in an approximate temperature of 11 K.

III. EXPERIMENTAL RESULTS AND ANALYSIS

A. Thermal gravimetric analysis

Figure 1 shows the TGA mass loss (in %) versus time for bulk $YBa_2Cu_3O_{7-\delta}$ with various fixed temperatures during deoxygenation. It can be seen that after 80 min, most of the deoxygenation has occurred. The TGA results yielded estimates for the nominal oxygen content or number of oxygen atoms per formula unit of $y\approx6.6$, 6.3, 6.2, and 6.1 after deoxygenation at fixed temperatures of 450, 550, 650, and 700 °C, respectively. These results were used to make the primary assignments for the nominal oxygen content of the deoxygenated samples listed in Table I. However, values obtained from XRD measurements of the lattice parameters and magnetization measurements of T_c were found to be in good agreement (see below in Sec. III C and III D, respectively).

B. Energy dispersive x-ray analysis

Energy dispersive x-ray analysis was used to monitor the Br atoms which were actually incorporated into the samples.

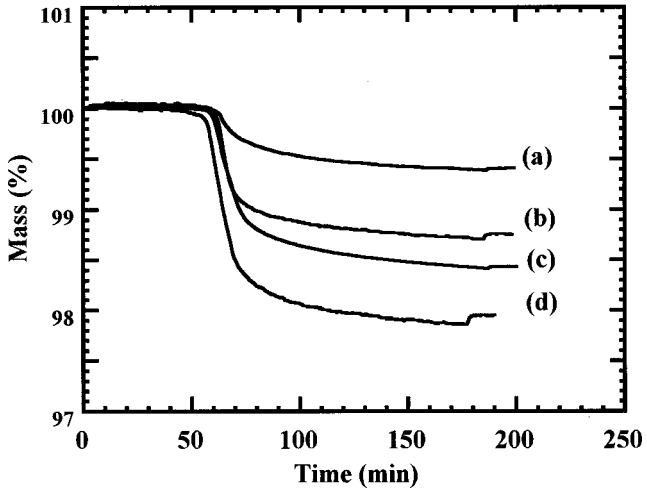

FIG. 1. Thermal gravimetric analysis measurement of the mass loss from bulk $YBa_2Cu_3O_{7-\delta}$ versus time during deoxygenation under He gas flow for various temperatures: (a) 450 °C, (b) 550 °C, (c) 650 °C, and (d) 700 °C.

The ratio of the Br-L_{I} to Y-L_{III} peak heights (at 1.5 and 1.8 keV, respectively) provided a quantitative comparison of the Br content between samples. For the three 1-μm $YBa_2Cu_3O_y$ samples which underwent the same bromination treatment (260 °C for $\frac{1}{2}$ h), the EDAX peak-height ratio was 0.1, 0.7, and 0.95 for S2, S4, and S6, respectively. Since sample S2 was not deoxygenated, the nominal oxygen content was $y \approx 6.9$. The oxygen content for sample S4, which was deoxygenated at 450 °C, was $y \approx 6.6$, while that for sample S6, which was deoxygenated at 700 °C was $y \approx 6.1$. The EDAX results clearly indicate a trend of increased bromine absorption into the samples for reduced oxygen content. This is also consistent with the EDAX results from the 30-μm samples which underwent bromination for 24 h. The peak ratio was 1.0 for sample M5 which was not deoxygenated, while the peak ratio was 3.6 for sample M6 which was deoxygenated at 700 °C for 4 h. The relatively large incorporation of Br into sample M6 is also apparent in the XRD pattern (see below).

C. X-ray diffraction

A series of typical XRD spectra obtained in this work are provided in Fig. 2. Figure 2(a) shows the standard Joint Committee on Powder Diffraction Standards (JCPDS) powder pattern for $YBa_2Cu_3O_{7-\delta}$.[16] Also shown are $YBa_2Cu_3O_y$ powder patterns for three of the 1-μm particle size samples: sample S1 which is the parent powder with $y = 7 - \delta \approx 6.9$ [Fig. 2(b)], sample S5 which was deoxygenated at 700 °C for 4 h yielding $y \approx 6.1$ [Fig. 2(c)], and sample S6 which was deoxygenated like sample S5 and brominated at 260 °C for $\frac{1}{2}$ h [Fig. 2(d)]. The Miller indices (*hkl*) for the principal YBCO peaks are indicated in Fig. 2(b). Listed in Table II are the orthogonal lattice parameters (*a*, *b*, and *c*) which were obtained by a least-squares fit of the peak positions, along with the unit-cell volume (V) and degree of orthorhombicity ($\mathrm{OR} = 200|(b-a)/(b+a)|$). The orthorhombic-tetragonal-orthorhombic shift is shown explicitly by the crystallographic data listed in Table II. In agreement with the results

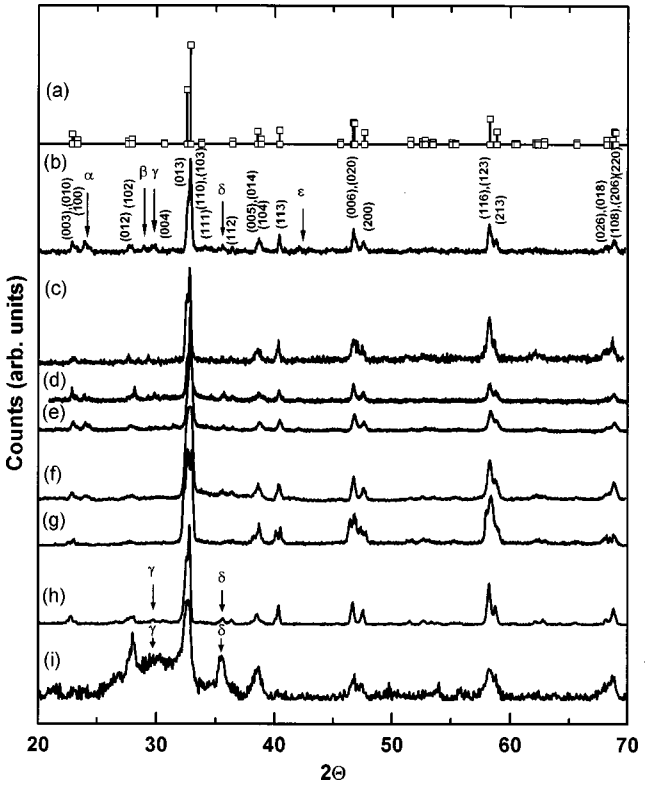

FIG. 2. X-ray-diffraction spectra obtained for the various $YBa_2Cu_3O_y$ samples: (a) standard JCPDS powder pattern for $YBa_2Cu_3O_{7-\delta}$, see Ref. 16; (b) sample S1, 1-μm particle size parent powder; (c) sample S5, 1-μm powder after deoxygenation at 700 °C for 4 h; (d) sample S6, 1-μm powder after deoxygenation at 700 °C for 4 h and bromination at 260 °C for $\frac{1}{2}$ h; (e) sample S4, 1-μm powder after deoxygenation at 450 °C for 4 h and bromination at 260 °C for $\frac{1}{2}$ h; (f) sample L3, 20-μm powder after deoxygenation at 450 °C for 4 h and bromination at 260 °C for $\frac{1}{2}$ h; (g) sample M3, 40-μm powder after deoxygenation at 450 °C for 4 h and bromination at 260 °C for $\frac{1}{2}$ h; (h) sample M5, 30-μm powder after only bromination at 260 °C for 24 h; and (i) sample M6, 30-μm powder after deoxygenation at 700 °C for 4 h and bromination at 260 °C for 24 h.

obtained by Radousky *et al.*,[2] the parent powder, which has an orthorhombic structure, becomes more tetragonal (lower OR) upon deoxygenation, and then returns to the more orthorhombic (higher OR) structure after bromination. The same trends were also observed for sample S3 which was deoxygenated at 450 °C for 4 h yielding $y \approx 6.6$ and sample S4 which was deoxygenated like sample S3 and brominated at 260 °C for $\frac{1}{2}$ h [Fig. 2(e)]. The crystallographic data also provide a measure of the oxygen stoichiometry for the various unbrominated samples as the lattice parameters can be directly related to the oxygen content.[17,18] A careful comparison of the lattice parameters for the deoxygenated samples S3 and S5 listed in Table II with the data of Cava *et al.*[18] supported the values assigned for the oxygen content from the TGA measurements. As seen in Fig. 2(b), there are some small peaks designated by α, β, γ, δ, and ε which are not associated with the YBCO crystal structure. These are due to a small amount of second phase(s) which came in with the parent powder. Likely candidates for the second phase(s) include $BaCO_3$, $BaCuO_2$, Ba_2CuO_3, Y_2O_3, CuO, and Cu_2O. Similar second phase peaks were observed for the 20-μm

TABLE II. Lattice constants for 1-μm powder samples.

Sample	a(Å)	b(Å)	c(Å)	V(Å)	OR
		Parent			
(S1) $YBa_2Cu_3O_{6.9}$	3.82(0)	3.87(5)	11.68(0)	172.(9)	1.4
		Deoxygenated			
(S3) $YBa_2Cu_3O_{6.6}$	3.83(0)	3.86(0)	11.74(5)	173.(6)	0.78
(S5) $YBa_2Cu_3O_{6.1}$	3.84(0)	3.85(0)	11.77(0)	174.(0)	0.26
		Deoxygenated and brominated			
(S4) $YBa_2Cu_3O_{6.6}$+Br	3.82(0)	3.88(0)	11.66(0)	172.(8)	1.6
(S6) $YBa_2Cu_3O_{6.1}$+Br	3.82(0)	3.87(0)	11.70(0)	172.(9)	1.0
		References values			
$YBa_2Cu_3O_{7-\delta}$[a]	3.819	3.886	11.680	173.3	1.7
$YBa_2Cu_3O_{6+\delta}$[b]	3.853	3.853	11.780	174.9	0

[a]Reference 16.
[b]Reference 17.

parent powder (L1); however, there was no trace of a second phase in the XRD patterns for the 30- and 40-μm parent powders (M4 and M1, respectively).

Figures 2(f) and 2(g) show the XRD powder patterns for the 20-μm (sample L3) and 40-μm (sample M3) particle size samples, respectively, which have both undergone deoxygenation at 450 °C for 4 h, and then bromination at 260 °C for $\frac{1}{2}$ h. The trend to return the more tetragonal (lower OR) structure to the more orthorhombic (higher OR) structure after bromination also occurred for the 20- and 40-μm samples; however, the 40-μm sample exhibited some additional peaks which were inconsistent with the $YBa_2Cu_3O_{7-\delta}$ structure. The additional peaks indicate the appearance of a second phase after bromination.[13]

Figure 2(h) shows the XRD powder pattern for the 30-μm sample M5 which was brominated at 260 °C for 24 h without undergoing a prior deoxygenation treatment, while Fig. 2(i) shows the pattern for the 30-μm sample M6 which was also brominated for 24 h like sample M5 after undergoing deoxygenation at 700 °C for 4 h. Although the parent powder sample for both of these samples showed no sign of any second phase peaks, such peaks start to appear for the samples after the long 24-h bromination time (γ and δ). Furthermore, sample M6 which was deoxygenated prior to the bromination treatment was altered more drastically than sample M5 which was not deoxygenated in that: (1) the YBCO peaks are broadened, (2) the second phase peaks are more intense, and (3) a broad background appears between 25° and 35°. A similar broad background also exists for sample M5; however, it is barely visible. The broad background is consistent with the existence of nanoscale-size regions of $BaBr_2$. It is noteworthy that the most intense peak in the XRD pattern for orthorhombic and hexagonal $BaBr_2$ occurs at 29.68° (121) and 30.59° (201), respectively.

D. Magnetization

Magnetization measurements were used to monitor the onset and fractional amount of superconductivity in the various parent, deoxygenated, and brominated samples (see Fig. 3). The zero-field-cooled (ZFC) magnetization versus temperature behavior $M(T)$ in emu/g was obtained for a fixed magnetic field intensity of $H=10$ Oe. Four parameters, which are listed in Table I, are defined to characterize the sample superconductivity: (1) $T_{\max}$, the temperature at which $M(T)$ has maximum slope, (2) T_c, the onset temperature for superconductivity, (3) $(M/M_p)_{10\ \mathrm{K}}$, the ZFC magnetization at $T=10$ K normalized by the value for the parent sample at 10 K, which provides a quantitative measure of the degree of suppression and restoration of superconductivity upon deoxygenation and bromination, respectively, and (4) MFR, the ZFC Meissner fraction. The Meissner fraction was calculated using $\mathrm{MFR}=(-)4\pi M\rho/H$, where ρ is the mass density. The small Meissner fraction of the parent materials S1 and L1 cannot be explained by the effect of penetration depth alone. However, grain boundaries containing nonstoichiometric material can strongly reduce the Meissner frac-

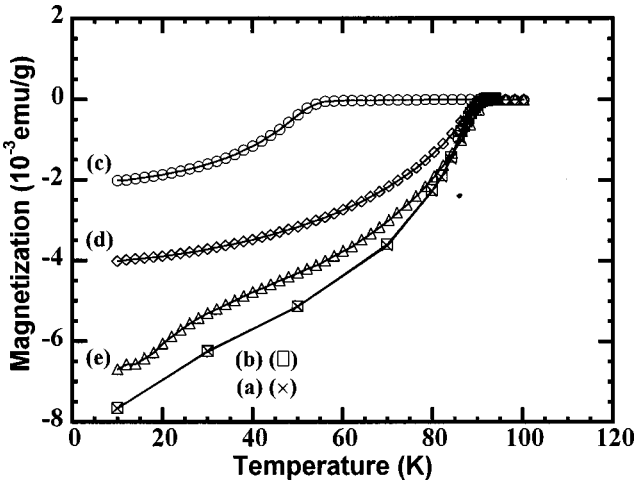

FIG. 3. Zero-field-cooled magnetization (in emu/g) versus temperature in a 10-Oe magnetic field for the various 1-μm particle size $YBa_2Cu_3O_y$ samples: (a) sample S1, parent powder; (b) sample S2, after only bromination at 260 °C for $\frac{1}{2}$ h; (c) sample S3, after deoxygenation at 450 °C for 4 h; (d) sample S4, after deoxygenation at 450 °C for 4 h and bromination at 260 °C for $\frac{1}{2}$ h; and (e) sample S9, after deoxygenation at 450 °C for 4 h and reoxygenation under O_2 flow at 560 °C for 4 h.

tion due to weakened coupling between grains within the particles, as reported in Clem[19] and Moodenbaugh *et al.*[20,21] The presence of small peaks due to such impurities were found in the x-ray diffraction data for samples S1 and L1, but not for the parent material from which M1 and M4 were derived.[13] From an inspection of the four superconductivity parameters in Table I, it can be seen for the 1-, 20-, and 40-μm samples that superconductivity was reduced in the samples deoxygenated at 450 °C (S3, L2, and M2) and completely suppressed (at least to $T=5$ K) in the samples deoxygenated at 700–750 °C (S5 and L4). The value of T_c for the parent and deoxygenated samples can also be used as a measure of the oxygen content in YBCO. For example, a consideration of the accepted relationship between carrier concentration (or oxygen content) and T_c for underdoped YBCO as provided by Birgeneau and Shirane[22] indicated that the values assigned for the oxygen content from the TGA measurements for the 1 and 20-μm samples (S3 and L2, respectively) were consistent, while that for the 40-μm sample (M2) might be an underestimate by a small amount. Also, from Table I, it can be seen that a subsequent bromination of the deoxygenated samples (S4, S6, L3, L5, and M3) resulted in partial restoration of the superconductivity in agreement with results reported previously.[2,3] In particular, $T_{\max}$ and T_c returned essentially to the parent values; however, $(M/M_p)_{10\ \mathrm{K}}$ returned to only a fraction of the parent value. The degree of restoration was smaller for the samples deoxygenated at higher temperature (700–750 °C) and having lower oxygen content. It is noteworthy that for the sample (S2) with no deoxygenation prior to the bromination treatment, both the superconducting transition temperature and fraction are essentially the same as for the parent sample (S1). Finally, for the 30-μm samples which underwent a long 24-h bromination, sample M5 with no deoxygenation prior to bromination showed essentially no change in the superconducting properties. However, sample M6 with prior deoxygenation showed a somewhat lower transition temperature and a drastically reduced superconducting fraction.

E. ^{63}Cu and ^{65}Cu nuclear quadrupole resonance and nuclear magnetic resonance

Detailed ^{63,65}Cu NQR studies (18–34 MHz) have been previously reported for nonbrominated $YBa_2Cu_3O_y$ with the oxygen content ranging from $y=7-\delta$ (superconducting phase) to $y=6+\delta$ (antiferromagnetic phase).[23–27] In addition, ^{63,65}Cu NMR studies also exist for the antiferromagnetic phase[28,29] over the frequency range 70–110 MHz. As described above, zero-field spin-echo NQR spectra were obtained in this work at 4.2 K over the frequency range 19.0–33.0 MHz. A series of spectra characteristic of the 1-μm particle size $YBa_2Cu_3O_y$ samples are presented in Fig. 4. Figure 4(a) shows the spectrum obtained for the parent ($y\approx 6.9$) powder sample S1 which is characterized by two pairs of peaks.[23,27] One pair at 20.5 and 22.1 MHz, which is attributed to ^{65}Cu and ^{63}Cu nuclei, respectively, results from the Cu(1) atoms in the CuO chains having four nearest-neighbor atoms with two O(4) atoms in the chains and two O(1) apical atoms. The second pair at 29.0 and 31.5 MHz, which is attributed to ^{65}Cu and ^{63}Cu nuclei, respectively, results from the Cu(2) atoms in the CuO_2 planes. The Cu(2)

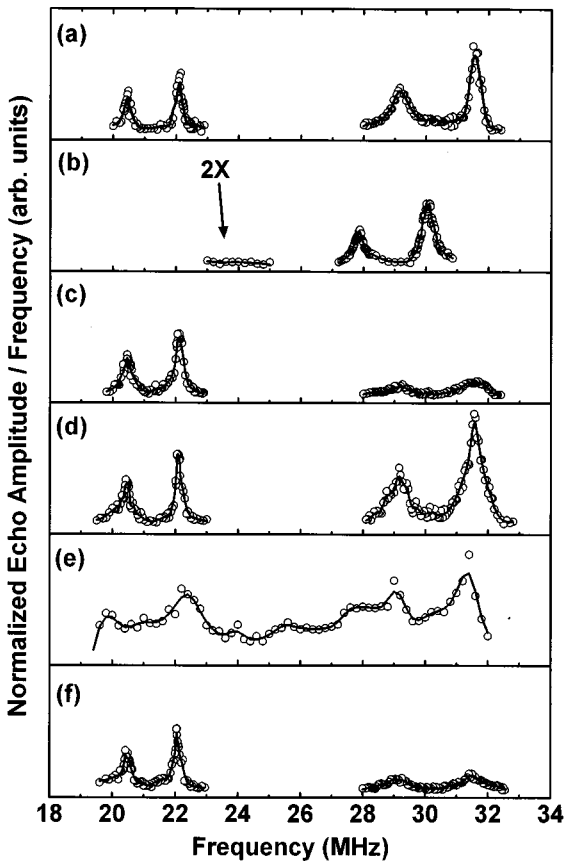

FIG. 4. ^{63,65}Cu spin-echo NQR spectra obtained at 4.2 K for various 1-μm particle size $YBa_2Cu_3O_y$ samples: (a) sample S1, parent powder; (b) sample S5, after deoxygenation at 700 °C for 4 h; (c) sample S6, after deoxygenation at 700 °C for 4 h and bromination at 260 °C for $\frac{1}{2}$ h; (d) sample S2, after only bromination at 260 °C for $\frac{1}{2}$ h; (e) sample S3, after deoxygenation at 450 °C for 4 h; and (f) sample S4, after deoxygenation at 450 °C for 4 h and bromination at 260 °C for $\frac{1}{2}$ h.

atoms have four nearest-neighbor oxygen atoms [two O(2) and two O(3)] and the symmetry is axial. There is significant deviation from axial symmetry for the Cu(1) atoms. Figure 4(b) shows the spectrum obtained from sample S5 which was deoxygenated at 700 °C for 4 h. It can be seen that the pair of peaks at 20.5 and 22.1 MHz associated with the Cu(1) atoms shift to 28.0 and 30.0 MHz, respectively. This is attributed to the two nearest-neighbor O(4) chain atoms being removed during the deoxygenation treatment.[23,24] Furthermore, the pair of peaks at 29.0 and 31.5 MHz, associated with the Cu(2) atoms, were observed in the 70–110 MHz range at 1.3 K (see Fig. 5 and discussion below), which is consistent with results reported previously for deoxygenated antiferromagnetic YBCO.[28,29] Also, Cu(1) peaks associated with the occupation of three nearest-neighbor oxygen sites [two O(1) and one O(4)] would appear in the 23.0- and 25.0-MHz range. As noted in Fig. 4(b), measurements in this range revealed no detectable signal indicating that the 700 °C deoxygenation essentially emptied the O(4) sites, one per unit cell. Figure 4(c) shows the spectrum obtained from sample S6 which was deoxygenated like sample S5 and brominated at 260 °C for $\frac{1}{2}$ h. At 260 °C, and without the presence of bromine, oxygen should not be able to return to the sample and restore the superconducting state. To confirm

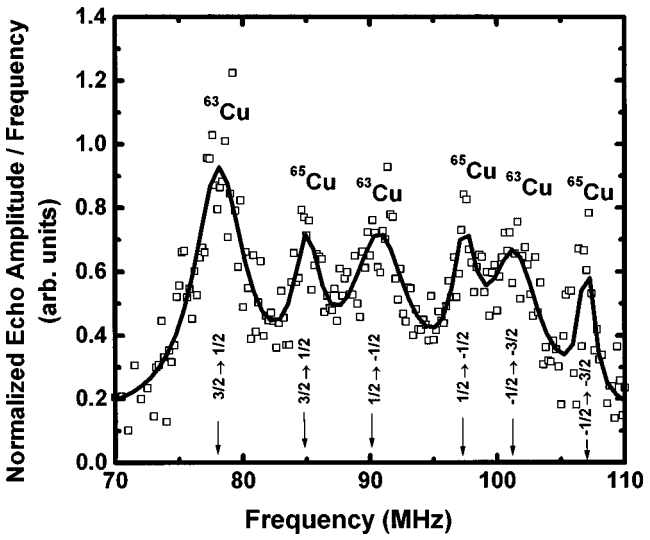

FIG. 5. ^{63,65}Cu zero-field spin-echo NMR spectra obtained at 1.3 K for the 1-μm particle size $YBa_2Cu_3O_y$ sample (S5) after deoxygenation at 700 °C for 4 h. The antiferromagnetic ordering results in a 79.47 ± 0.04 kOe hyperfine field at the Cu(2) sites along with the quadrupolar splitting of 23.00 and 22.10 MHz for ^{63}Cu and ^{65}Cu, respectively.

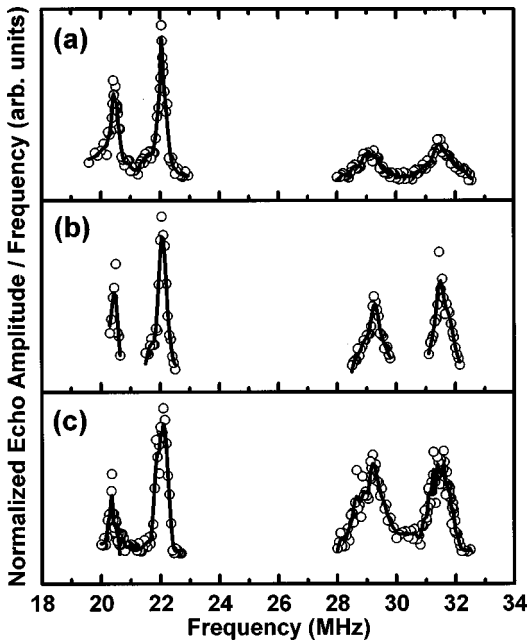

FIG. 6. ^{63,65}Cu spin-echo NQR spectra obtained at 4.2 K for various particle size $YBa_2Cu_3O_y$ samples after deoxygenation at 450 °C for 4 h and bromination at 260 °C for $\frac{1}{2}$ h; (a) sample S4, 1 μm, (b) sample L3, 20 μm, and (c) sample M3, 40 μm.

this, a deoxygenated YBCO sample was held at 260 °C for $\frac{1}{2}$ h in the evacuated bromination chamber (without introducing Br). NQR measurements before and after the treatment showed no change, i.e., the spectra for samples S7 and S8 were identical. Bromination restores the pair of peaks associated with the Cu(1) atoms to 20.5 and 22.1 MHz (four nearest-neighbor oxygen atoms), suggesting that oxygen returns to the O(4) chain sites. This could be due to redistribution of the oxygen in the sample after the bromination treatment, and could account for the partial restoration of superconductivity observed in the magnetometer results (a model is presented in Sec. IV). In addition, there is a reappearance of the pair of peaks at 29.0 and 31.5 MHz associated with the Cu(2) atoms; however, their width is broadened and intensity is significantly reduced relative to those in a typical YBCO superconductor such as the parent sample S1. This suggests that the local coordination around the Cu has been perturbed. Unlike the deoxygenated sample S5, no Cu(2) peaks were observed in the 70–110 MHz range for the brominated sample S6. Figure 4(d) shows the spectrum for sample S2, which was the parent powder (S1) subjected only to the bromination treatment. It is essentially identical to the spectrum for the parent sample S1, except for a small broadening of the peaks. It can be seen that bromination alone does not result in the severe reduction in the intensity of the Cu(2) peaks.

Figure 4(e) shows the spectrum obtained on sample S3 which was deoxygenated at 450 °C for 4 h. The appearance of several weak and broad peaks indicates the partial removal of oxygen. There are ^{65,63}Cu peaks at 20.5 and 22.1 MHz attributed to Cu(1) atoms with two O(4) nearest neighbors, and at 29.0 and 31.5 MHz attributed to Cu(2) atoms when the two O(4) sites [second-near O(4) neighbors relative to Cu(2)] are filled; this situation indicates regions of the sample where the oxygen content is $y = 7 - \delta$. There are also peaks at 28.0 and 30.0 MHz attributed to Cu(1) atoms with zero O(4) nearest neighbors, characteristic of sample regions where $y \approx 6.0$. In addition, there are peaks in the 23.0 and 25.0 MHz range attributed to Cu(1) atoms with one O(4) nearest-neighbor indicating sample regions with intermediate oxygen content. Finally, Fig. 4(f) shows the spectrum obtained on sample S4 which was deoxygenated at 450 °C like sample S3 and brominated at 260 °C for $\frac{1}{2}$ h. Again, it can be seen that bromination restores the peaks to the parent (S1) values with the Cu(2) peaks being broadened and significantly reduced in intensity.

Following deoxygenation at 700 °C, sample S5 is antiferromagnetic. The two ^{65,63}Cu peaks attributed to Cu(2) atoms, that were present at 29.0 and 31.5 MHz prior to deoxygenation are shifted to a higher frequency range (70–110 MHz) as shown in Fig. 5. In agreement with previously reported results for similarly deoxygenated samples, the antiferromagnetic interaction results in a local hyperfine field at the Cu(2) sites of 79.47 ± 0.04 kOe along with a quadrupolar splitting of 23.00 and 22.10 MHz for ^{63}Cu and ^{65}Cu, respectively.[28,29] Upon bromination (sample S6), these high frequency peaks completely disappear. The spectra for three samples with different particle size, S4 (1μm), L3 (20 μm), and M3 (40 μm), are compared in Figs. 6(a), (b), and (c), respectively. The three samples have undergone identical deoxygenation (450 °C for 4 h) and bromination (260 °C for $\frac{1}{2}$ h) treatments. As was the case for the 1-μm sample (S4) described above, the Cu(1) and Cu(2) peaks returned to the parent values upon bromination for both the 20-μm (L3) and 40-μm (M3) samples. Again, the Cu(2) peaks were broadened and reduced in intensity. However, it can be seen that, relative to the Cu(1) peaks, the Cu(2) peaks increased in intensity as the particle size increased. As mentioned above, magnetometry measurements of T_c indicated that the 40-μm sample was slightly less deoxygenated (slightly larger oxygen content) than the 1 and 20-μm samples. The shapes of the Cu(2)

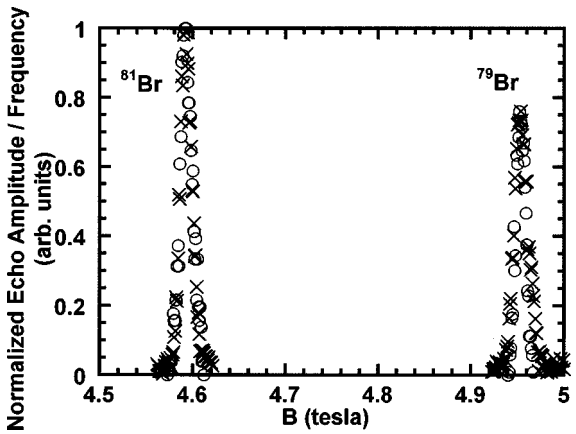

FIG. 7. ^{79,81}Br spin-echo NMR spectra obtained at 295 K for fixed frequency $\nu = 52.84$ MHz: ($\times$) $BaBr_2$ powder, (O) sample S6, 1-μm particle size $YBa_2Cu_3O_y$ after deoxygenation at 700 °C for 4 h and bromination at 260 °C for $\frac{1}{2}$ h.

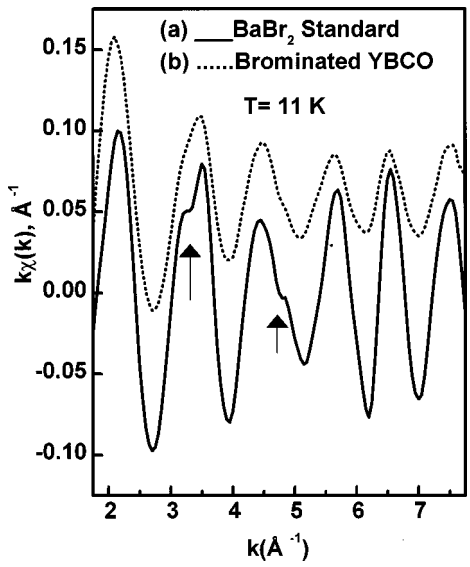

FIG. 8. Comparison of the Br *K*-edge XAFS, $k\chi(k)$, taken at 11 K: (a) $BaBr_2$ (solid line) and (b) sample S6 (broken line), 1-μm particle size YBCO, after deoxygenation at 700 °C for 4 h and bromination at 260 °C for $\frac{1}{2}$ h.

peaks for the various particle size samples also suggest the possibility of a coexistence of a broad contribution from a component whose Cu(2) environment has been perturbed and a sharp contribution reminiscent of plane sites in a well-ordered superconductor.

F. ^{79}Br and ^{81}Br nuclear magnetic resonance

Figure 7 shows the (normalized) ^{79,81}Br spin-echo NMR spectrum obtained at room temperature (295 K) for the 1-μm particle size $YBa_2Cu_3O_y$ sample (S6), which was deoxygenated at 700 °C for 4 h and brominated at 260 °C for $\frac{1}{2}$ h. At 295 K, the sample is in the normal state. For 52.84 MHz, the values for $\gamma(^{79}\mathrm{Br}) = 10.667$ MHz/T and $\gamma(^{81}\mathrm{Br}) = 11.498$ MHz/T correspond to (unshifted) resonance peaks at 4.953 T and 4.596 T, respectively. For comparison, the corresponding ^{79,81}Br NMR spectrum was measured for $BaBr_2$ powder (see Fig. 7). The positions of the peaks for the two spectra are the same; the accuracy of the measurement dictates that any NMR shift of the sample relative to $BaBr_2$ is $\leq 0.06\%$. The quadrupole structure for the ^{79,81}Br lines was not resolved.

G. Br *K*-edge x-ray-absorption fine structure

Information concerning the local structure of bromine was obtained by measurements of the Br *K*-edge XAFS on sample S6 as well as $BaBr_2$ powder. Because the room-temperature and 200 K XAFS data on the Br showed very weak modulations of the absorption, a commercially available Displex refrigerator was used to cool the sample to 11 K, thus obtaining satisfactory XAFS spectra over sufficiently wide *k* range. Data reduction consisted of pre-edge and post-edge background subtraction, step-normalization at the edge, extraction of the XAFS $\chi(k)$ function, and subsequent Fourier transform (FT) from *k* to *r* space. The extraction of $\chi(k)$ and the FT spectra were performed using the AUTOBK and FEFFIT routines, respectively, in the UWXAFS 3.0 package.[30] Figure 8 shows a comparison of the *k*-weighted $\chi(k)$ function of Br obtained at 11 K for sample S6 and the $BaBr_2$ standard. The photoelectron wave vector *k* is given by $k = [2m(E-E_0)]^{1/2}/\hbar$, where *E* is the energy of the x-ray photon, E_0 is the threshold energy, and *m* is the mass of the electron. Five individual scans were averaged for sample S6 and two scans were averaged for $BaBr_2$ to improve the signal-to-noise ratio. The primary frequency oscillations for sample S6 and the $BaBr_2$ are in phase, suggesting that the immediate near-neighbor environment around Br in sample S6 is similar to that of $BaBr_2$. The intensity of the oscillations is much larger for $BaBr_2$ compared to sample S6 throughout the entire *k* range. Due to the backscattering nature of the atoms surrounding Br in $BaBr_2$, the XAFS signal also has a minimum near 4.5 Å^{-1} (see Fig. 8). At room temperature, the thermal excitation of the lattice vibrations in $BaBr_2$ is substantial due to the low Debye temperature[31] and contributes to the large thermal disorder which causes the XAFS signal to dampen significantly. This factor contributes to a significant reduction in the XAFS signal beyond 4.5 Å^{-1} for sample S6 at room temperature as well. However, at 11 K, the only contribution to thermal disorder comes from the zero-point motion, and appreciable signal out to larger *k* values ($\sim$8 Å^{-1}) can be obtained. The reduction in amplitude of the XAFS oscillations for sample S6 compared to $BaBr_2$ shown in Fig. 8 can be due to either disorder, σ^2, or reduction in the coordination number. Disorder enters into the XAFS expression as a decay term, $\exp(-2k^2\sigma^2)$, while the coordination number has no *k* dependence. The large reduction in the XAFS amplitude throughout the entire *k* range suggests that the average coordination number around Br in sample S6 is smaller than that in $BaBr_2$. Also, it can be seen that the high-frequency modulations (indicated by arrows in Fig. 8), which arise due to contributions from relatively long scattering paths (both single scattering as well as multiple scattering), are much weaker in sample S6 when compared to $BaBr_2$. This suggests that the contributions of the longer scattering paths are diminished in brominated YBCO.

A quantitative analysis of the XAFS spectra is obtained by Fourier transformation. Figures 9(a) and 9(b) show the magnitude and imaginary part of the *k*-weighted FT spectra,

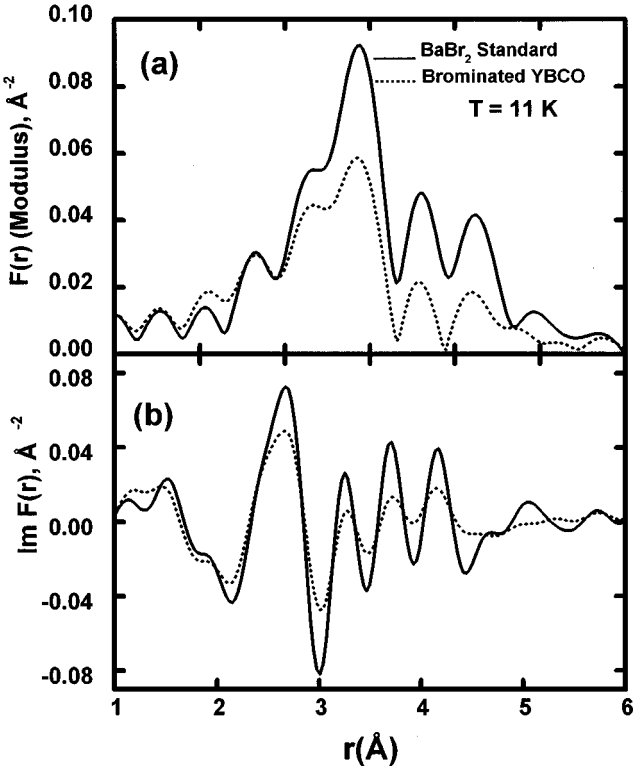

FIG. 9. Comparison of Fourier transform of $k\chi(k)$ for the Br *K*-edge XAFS taken at 11 K, for $BaBr_2$ (solid line) and YBCO after deoxygenation and bromination (sample S6) (broken line): (a) modulus and (b) imaginary part.

respectively, for both sample S6 and $BaBr_2$ at 11 K. The general appearance of the FT spectra are similar out to ~4.5 Å, clearly illustrating that the local environment around Br is similar. The peak heights for $BaBr_2$ are much larger than for sample S6. If Br precipitates as small particles of $BaBr_2$ in brominated YBCO, a reduction in peak heights can be expected. Br atoms on the surface of the small precipitates have a smaller number of near neighbors, resulting in reduced coordination number. Under favorable conditions, detailed fitting analysis of the XAFS spectra (including information up to the third or fourth coordination shell) can be utilized to determine the size and morphology of the precipitate.[32] In $BaBr_2$, Br occupies two inequivalent sites with a large distribution of neighboring Br-Ba and Br-Br distances about each site as tabulated in Brackett *et al.*[33] The information that can be extracted from the XAFS spectra by nonlinear fitting to standards is governed by Brillouin's theorem, and consequently the XAFS data is bandwidth limited.[34] Due to the complexity of the local structure surrounding Br in $BaBr_2$, a detailed fitting of the XAFS of Br in brominated YBCO would require too many adjustable variables and hence would be indeterminate. A reasonable estimate from the diminution of the peak heights in the FT spectra suggests that the particle size is in the 10–20 Å range. In a neutron-diffraction study of Br-doped YBCO, Mokhtari *et al.*[4] suggested that Br occupies the vacant O(4) sites in the YBCO lattice. As mentioned earlier, room-temperature measurements show negligible signal past ~4.5 $Å^{-1}$. Br in the O(4) sites will be coordinated to the Cu, Y, and Ba atoms of the YBCO lattice. These elements are strong backscatterers of the photoelectrons in the high *k* region. Hence the absence of signal past ~4.5 $Å^{-1}$ in the room-temperature data reveals that no Br atoms occupy the YBCO lattice. An inspection of the neutron-diffraction data and analysis shows that the possibility of $BaBr_2$ precipitates was not included in the Reitveld refinement.[4] Furthermore, our XAFS data suggest that the precipitates are small and hence may be difficult to detect in the diffraction data. It should be noted that the element-specific nature of the XAFS technique reveals the local structure around the Br atoms exclusively and is insensitive to long-range order. This allows it to complement the results of any conventional diffraction techniques in such complex and important materials.

IV. DISCUSSION AND CONCLUSIONS

In this work, deoxygenated and brominated $YBa_2Cu_3O_y$ powder with 1-, 20-, 30-, and 40-μm particle size were studied using ^{63,65}Cu NQR and NMR, ^{79,81}Br NMR, and Br *K*-edge XAFS measurement techniques. The samples were characterized with a combination of XRD, TGA, and SQUID magnetometry. TGA measurements on bulk $YBa_2Cu_3O_{7-\delta}$ indicated that a nominal oxygen content of $y=6.6$, 6.3, 6.2, and 6.1 results when the deoxygenation is carried out for 4 h at 450, 550, 650, and 700 °C, respectively, as a consequence of oxygen atoms leaving the O(4) sites. Estimates for the oxygen content in the powder samples after deoxygenation, which were obtained from the XRD and magnetometry measurements, are consistent with the above results on bulk specimens. There was an indication that the larger particle size sample (40 μm) has a slightly larger oxygen content after deoxygenation at 450 °C than the 1- and 20-μm samples. Also, as indicated by XRD and SQUID magnetometry measurements, the orthorhombic YBCO structure becomes more tetragonal and the superconductivity is suppressed after deoxygenation. Upon bromination, the YBCO structure is returned from the tetragonal phase to the orthorhombic phase with superconductivity being partially restored. All of the above characteristics are consistent with previous studies.[1–4]

A microscopic picture of the deoxygenation/bromination process was obtained from the ^{63,65}Cu NQR and NMR spectra for the various samples. For the 1-μm particle size $YBa_2Cu_3O_y$ powder deoxygenated at 700 °C for 4 h, the pair of peaks at 20.5 and 22.1 MHz, which is attributed to ^{65}Cu and ^{63}Cu nuclei, respectively, and results from the Cu(1) atoms in the CuO chains, is completely shifted to 28.0 and 30.0 MHz. Furthermore, a second pair of peaks at 29.0 and 31.5 MHz, which is attributed to ^{65}Cu and ^{63}Cu nuclei, respectively, and results from the Cu(2) atoms in the planes, is observed in the 70–110 MHz range. These results indicate that for 700 °C, the deoxygenation is essentially complete and approximately one O(4) atom is removed per YBCO unit cell [two of the four nearest neighbors for Cu(1)]. Deoxygenation at 450 °C results in a partial removal of the O(4) atoms as indicated by the presence of Cu(1) and Cu(2) peaks characteristic of both ''fully deoxygenated'' ($y=6+\delta$) and ''fully oxygenated'' ($y=7-\delta$) YBCO as well as peaks characteristic of intermediate oxygen content in the 23–25 MHz range. Bromination at 260 °C for $\frac{1}{2}$ h restores the Cu(1) and Cu(2) peaks for the fully deoxygenated and partially

deoxygenated ($y \approx 6.6$) 1-μm YBCO powder to the frequencies associated with the fully oxygenated parent powder. However, the heights of the plane Cu(2) peaks are diminished relative to the chain Cu(1) peaks in the brominated samples compared to those in the parent material. This suggests that there may be a distortion in the local structure near the Cu(2) sites. Furthermore, the shape of the Cu(2) peaks in the NQR spectra also suggests the possibility of a coexistence of a broad contribution from a component whose Cu(2) environment has been perturbed and a sharp contribution reminiscent of the plane sites in a well-ordered parent material. Similar results were obtained for the 20- and 40-μm particle size samples, i.e., bromination restored the Cu(1) and Cu(2) NQR peaks to the parent peak frequency values. However, the Cu(2) peaks exhibited an increase in height relative to the Cu(1) peaks with increased particle size. The restoration of the Cu(1) and Cu(2) spectra is attributed to oxygen being returned to (rather than bromine entering into) the O(4) chain sites of the YBCO structure. It is evident that the equilibrium bromine procedure employed in this work uses a temperature (260 °C) which is too low and/or a time ($\frac{1}{2}$ h) which is too short for oxygenation to occur without the presence of bromine. The spectra obtained from previously deoxygenated samples before and after a $\frac{1}{2}$ h treatment at 260 °C (without the introduction of bromine) were essentially the same; there was no restoration of the Cu(1) and Cu(2) peaks. The similarity of the two spectra indicates negligible intergranular mobility at this temperature (260 °C) in YBCO.[35,36] This result underscores the importance of bromine in the creation of the proper conditions for the restoration of the ^{63,65}Cu NQR spectrum and, correspondingly, the superconductivity. Finally, a comparison of the NQR spectra for a fully oxygenated parent material before and after bromination revealed no significant differences, indicating that the bromination procedure has little or no effect on the fully oxygenated YBCO material.

Additional evidence for the kinds of reactions occurring and the products formed during the bromination procedure is provided by the low-temperature XAFS measurements of the Br *K*-edge for the deoxygenated and brominated 1-μm YBCO powder sample. These results demonstrate that Br does not occupy any detectable number of sites within the YBCO lattice, either as a substitutional or an interstitial atom. Instead, there is a precipitation of nanoscale-size particles of $BaBr_2$. This is also supported by the ^{79,81}Br NMR results which show that the local environment surrounding the Br in the deoxygenated and brominated 1-μm YBCO sample is similar to that in $BaBr_2$ powder. Since the NQR for copper is broadened and distorted, further efforts to explore the local distribution about the Cu site using XAFS are currently underway. In an attempt to draw out the phase products which are produced during the bromination treatment, a deoxygenated sample was brominated at 260 °C for an extended time (24 h). The XRD spectra from this sample revealed a broad amorphouslike peak appearing in the 25°–35° range (Cu $K\alpha$ radiation) which could be attributed to $BaBr_2$ with small particle size. Also, a strong peak appears at 35.5° which is consistent with the most intense peak of tenorite (CuO). The magnetometer results for field-dependent magnetization indicate the corresponding appearance of a small paramagnetic component upon prolonged bromination. Likely candidates for a paramagnetic reaction product whose strongest x-ray-diffraction peaks would also appear in the 25°–35° range would be CuO, Y_2O_3, and $BaCuO_2$.[37]

A sequence of events may now be proposed which describes the changes observed upon bromination in deoxygenated YBCO. The bromine creates a local decomposition of the deoxygenated YBCO (Ref. 38) and, in the process, reacts with barium to form barium bromide precipitates with nanoscale dimensions. As a consequence of the decomposition reaction, oxygen is liberated, which is then available to reoxygenate the local regions of deoxygenated YBCO that have not undergone decomposition and, in doing so, partially restores superconductivity. The presence of a low density of very small local regions of decomposition would explain the reduction in the critical current for the brominated YBCO compared to the parent material. Very recently, experimental studies of Goren *et al.*[39] indicated that the halogens F and Cl enter the YBCO lattice in compounds prepared using NF_3 and CCl_4, respectively, diluted in N_2. They suggest that for diluted gaseous bromine compounds, where reaction conditions are milder than in the direct reaction with Br_2, the bromine may be able to enter the YBCO lattice.

ACKNOWLEDGMENTS

We wish to acknowledge useful discussions with Ch. Bernhard, W. G. Clark, D. M. Pease, H. B. Radousky, R. Stern, R. E. Walstedt, and Y. D. Zhang. We wish to thank M. Daniel for assistance with XAFS measurements and AFR, Inc. for collaboration in the initial bromination experiments. The work at the University of Connecticut received funding from Connecticut Critical Technologies Grant No. CII(93G049), Department of Energy Grant No. DE-FG05-89-ER45384, and, in the initial stages of experimentation, from AFOSR-SBIR Grant No. F49620-93-C-0010. Research at Brookhaven is supported by the U.S. Department of Energy, Office of Basic Energy Sciences, Division of Materials Sciences, under Contract No. DE-AC02-98-CH10886.

*Present address: Epion Corp., Billerica, MA 01821.

[1] E. B. Amitin, N. V. Bausck, S. A. Gromilov, S. G. Kozlova, N. K. Moroz, L. N. Mazalov, V. N. Naumov, P. P. Samoilov, S. A. Slobodjan, M. A. Starikov, V. E. Fedorov, G. I. Frolova, and S. B. Erenburg, Physica C **209**, 407 (1993).

[2] H. B. Radousky, R. S. Glass, P. A. Hahn, M. J. Fluss, R. G. Meisenheimer, B. P. Bonner, C. I. Mertzbacher, E. M. Larson, K. D. McKeegan, J. C. O'Brien, J. L. Peng, R. N. Shelton, and K. F. McCarty, Phys. Rev. B **41**, 11 140 (1990).

[3] P. P. Nguyen, Z. H. Wang, A. M. Rao, M. S. Dresselhaus, J. S. Moodera, G. Dresselhaus, H. B. Radousky, R. S. Glass, and J. Z. Liu, Phys. Rev. B **48**, 1148 (1993).

[4] M. Mokhtari, C. Perrin, M. Sergent, E. Furet, J. F. Halet, J. Y. Saillard, E. Ressouche, and P. Burlet, Solid State Commun. **93**,

487 (1995).
[5] D. B. Fenner, J. I. Budnick, D. M. Potrepka, Q. Li, P. A. Rosenthal, J. Luo, and W. D. Hamblen, IEEE Trans. Appl. Supercond. **5**, 3397 (1995).
[6] D. M. Potrepka, M. Balasubramanian, D. B. Fenner, W. A. Hines, and J. I. Budnick, Appl. Phys. Lett. **73**, 1137 (1998).
[7] M. Mokhtari, C. Perrin, O. Peña, and M. Sargent, Physica C **202**, 141 (1992).
[8] Contract No. F49620-93-C-0010, from DOD-BMDO, administered by AFOSR, technical monitor Dr. Harold Weinstock, work at Advanced Fuel Research, East Hartford, Connecticut, principal investigator D. B. Fenner.
[9] Y. Fukuda, N. Sanada, Y. Suzuki, T. Goto, M. Nagoshi, Y. Syono, and M. Tachiki, Phys. Rev. B **47**, 418 (1993).
[10] E. Kemnitz, T. Olesh, N. Pruss, A. Simon, H. Mattausch, R. K. Kremer, and W. Bauhofer, Mater. Res. Bull. **25**, 1019 (1990).
[11] E. Faulques, P. Mahot, M. Spiesser, T. P. Nguyen, G. Garz, C. Gonzalez, and P. Molinié, Phys. Rev. B **50**, 1209 (1994).
[12] D. E. Cox, A. R. Moodenbaugh, J. J. Hurst, and R. H. Jones, J. Phys. Chem. Solids **49**, 47 (1988).
[13] D. M. Potrepka, Ph.D. thesis, University of Connecticut, 1998.
[14] J. C. Ford, Ph.D. thesis, University of Connecticut, 1988.
[15] D. Brewe, Ph.D. thesis, University of Connecticut, 1993.
[16] W. Wong-Ng, H. McMurdie, B. Paretzkin, C. Hubbard, and A. Dragoo, Powder Diffraction File No. 38-1433, JCPDS–International Center for Diffraction Data, Newtown Square, PA (1987).
[17] P. K. Gallagher, H. M. O'Bryan, S. A. Sunshine, and D. W. Murphy, Mater. Res. Bull. **22**, 995 (1987).
[18] R. J. Cava, A. W. Hewatt, E. A. Hewat, B. Batlogg, M. Marezio, K. M. Rabe, J. J. Krajewski, W. F. Peck, Jr., and L. W. Rupp, Jr., Physica C **165**, 419 (1990).
[19] J. R. Clem, Physica C **153-155**, 50 (1988).
[20] A. R. Moodenbaugh, U. Wildgruber, Y. L. Wang, and Y. Xu, Physica C **245**, 347 (1995).
[21] A. R. Moodenbaugh, L. H. Lewis, and S. Soman, Physica C **290**, 98 (1997).
[22] R. J. Birgeneau and G. Shirane, *Physical Properties of High Temperature Superconductors I*, edited by D. M. Ginsburg (World Scientific, Singapore, 1989), p. 151.
[23] A. J. Vega, W. E. Farneth, E. M. McCarron, and R. K. Bordia, Phys. Rev. B **39**, 2322 (1989).
[24] H. Lütgemeier, Physica C **153-155**, 95 (1988).
[25] I. Heinmaa, H. Lütgemeier, S. Pekker, G. Krabbes, and M. Buchgeister, Appl. Magn. Reson. **3**, 689 (1992).
[26] M. Mali, D. Brinkmann, L. Pauli, J. Roos, H. Zimmerman, and J. Hulliger, Phys. Lett. A **124**, 112 (1987).
[27] C. P. Poole, Jr., H. A. Farach, and R. J. Creswick, *Superconductivity* (Academic, San Diego, 1995).
[28] H. Yasuoka, T. Shimizu, Y. Ueda, and K. Kosuge, J. Phys. Soc. Jpn. **57**, 2659 (1988).
[29] P. Mendels and H. Alloul, Physica C **156**, 355 (1988).
[30] E. A. Stern, D. F. Sayers, and F. W. Lytle, Phys. Rev. B **11**, 4836 (1975).
[31] S. Peng and G. Grimvall, J. Phys. Chem. Solids **55**, 707 (1994).
[32] R. B. Greeger and F. W. Lytle, J. Catal. **63**, 476 (1980).
[33] E. B. Brackett, T. E. Brackett, and R. L. Sass, J. Phys. Chem. **67**, 2132 (1963).
[34] E. A. Stern, Phys. Rev. B **48**, 9825 (1993).
[35] G. W. Morris, E. J. Tomlinson, R. E. Somekh, Z. H. Barber, E. J. Williams, M. P. Ray, and J. E. Evetts, IEEE Trans. Magn. **27**, 1430 (1991).
[36] W. E. McKinnon, M. L. Post, L. S. Selwyn, and G. Pleiaier, Phys. Rev. B **38**, 6543 (1988).
[37] H. M. Seyoum, M. Melamud, W. Wong-Ng, L. H. Bennett, L. J. Swartzendruber, L. Cook, and H. J. Brown, J. Appl. Phys. **81**, 4244 (1997).
[38] M. Mokhtari, O. Peña, A. Perrin, and M. Sergent, Mater. Lett. **13**, 241 (1992).
[39] S. D. Goren, L. Frenkel Ben-Yakar, A. Shames, B. Pandyopadhayay, C. Korn, H. Shaked, P. Massiot, C. Perrin, J. Gallier, and A. Privalov, Physica C **313**, 127 (1999).